THE ASTROPHYSICAL JOURNAL, 449:554–566, 1995 August 20

ROSAT OBSERVATIONS OF DISTANT CLUSTERS OF GALAXIES

MEGAN DONAHUE
Space Telescope Science Institute, 3700 San Martin Drive, Baltimore, MD 21218; donahue@stsci.edu
AND
JOHN T. STOCKE
Center for Astrophysics and Space Astronomy, CB391, University of Colorado, Boulder, CO 80309-0391; stocke%hyades@vaxf.colorado.edu
Received 1994 November 10; accepted 1995 March 7

ABSTRACT

We present the results of *ROSAT* Position Sensitive Proportional Counter and High Resolution Imager observations of two distant clusters of galaxies, MS 0735+74 and MS 0451−03, selected from the *Einstein* Extended Medium-Sensitivity Survey (EMSS). The cluster MS 0735+74 at $z = 0.216$ is a cooling flow candidate because the central brightest galaxy has extended Hα emission. We present optical spectra and a radio map for this cluster's brightest cluster galaxy. MS 0451−03, at a newly determined redshift of $z = 0.55$, is the most luminous cluster in the EMSS with $L_x(0.5\text{–}3.5\ \text{keV}) = 2.0 \times 10^{45}$ ergs s^{-1} h_{50}^{-2}. We derive significant limits on gas temperatures in these clusters and measure their core radii, "β_{image}," and mass cooling rates. We estimate gas masses and total gravitational masses for each cluster. We quantify structure by fitting isophotal ellipses and by decomposing the images with a wavelet analysis. The clusters are elliptical, but we measure no other significant substructure. In the cluster MS 0735+74 we compare the structure and flux from the central optical emission-line nebulosity to the cluster's X-ray and radio emission from the same region. We discuss the significance of the measured X-ray properties in the context of cluster evolution and cooling flows. Our results show that "cooling flows" can be identified by their extended Hα emission and that distant clusters probably do not have more intrinsic absorption than nearby clusters. We suggest that these distant clusters have X-ray morphologies similar to those of rich nearby clusters and that MS 0451−03, a luminous cluster at high redshift, may have somewhat lower $M_{\text{gas}}/M_{\text{total}}$ ratios ($\lesssim$17% at 1 h_{50}^{-1} Mpc scales) than low-redshift clusters of comparable luminosity.

Subject headings: cooling flows — galaxies: clusters: individual (MS 0735+74, MS 0415−03) — X-rays: galaxies

1. X-RAYS FROM DISTANT CLUSTERS AND CLUSTER EVOLUTION

Clusters of galaxies are continuing to form at the present epoch, and their outskirts are still collapsing linearly. The most distant clusters are the most likely to show evidence of evolution in structure, temperature, and X-ray luminosity. We already know that the X-ray luminosity function (LF) of distant clusters differs from that of nearby clusters (Gioia et al. 1990a; Edge et al. 1990; Henry et al. 1992) in the sense that there are fewer distant clusters with high X-ray luminosities than there are locally. This result tells us that clusters evolve significantly between $z \sim 0.3$ to the present but does not tell us how the evolution occurs. Evolution of the X-ray luminosity function may be caused by temperature evolution (or evolution of the L_x-T_x relation), by gas density evolution, by changes in the absorption by gas intrinsic to the clusters, or by incremental luminosity enhancements as small clusters merge to form large ones. Here, we report the results of *ROSAT* observations of two distant clusters that show how the X-ray properties of individual distant clusters might differ from those of similar nearby, X-ray clusters.

Since the hot gas in clusters responds to the cluster gravitational potential, in the absence of any dramatic merger shocks (Burns et al. 1994; Roettiger, Burns, & Loken 1993), the temperature of the hot gas is an adequate measure of the gravitational binding energy in the system (Evrard 1990; Tsai, Katz, & Bertschinger 1994). X-ray maps of surface brightness can reveal variations in the hot gas density. As the depth of the X-ray observation increases, our view of the X-ray cluster substructure and gravitational potential improves as X-ray photons are accumulated. In contrast, counting galaxies to define cluster structure is limited ultimately by the number of galaxies in the system. In the presence of merger compression or shocks, the hot gas may depart from hydrostatic equilibrium and reflect the hydrodynamics of a merger.

Measuring baryonic fractions in condensed systems and providing insights into the production of dark baryons and the origin and state of the intracluster medium (ICM) are possible with X-ray observations of distant clusters. Since X-rays directly count the baryons in hot gas and hot baryons are the dominant *luminous* mass component of rich clusters ($M_{\text{gas}} \sim 3\text{–}5M_{\text{galaxies}}$; David, Forman, & Jones 1990; Arnaud et al. 1992b; Edge & Stewart 1991b), X-ray observations are crucial for measuring cluster mass-to-light ratios (M/L). Cluster X-rays directly count the baryons in the hot gas since the emissivity of hot gas is much more sensitive to the density than to the temperature ($\propto T_x^{1/2} n_e^2$). At least for clusters at low redshift, the high gas–to–total mass ratios observed are incompatible with baryonic limits placed by cosmic nucleosynthesis and a flat universe (see White et al. 1993.) The $M_{\text{gas}}/M_{\text{total}}$ ratio in clusters of galaxies may be lower for galaxies at high redshift if delayed infall is a significant process in cluster evolution (Kaiser 1991). Gaseous dark matter may pool in the centers of clusters (Thomas & Fabian 1990). Such gas may affect a cluster's appearance by absorbing soft X-rays and may alter the derivation of the distribution and magnitude of cooling

flow gas in the cluster if the absorbing gas has sufficient optical depth and covering fraction (Wise & Sarazin 1993; White et al. 1991).

In this paper, we report on *ROSAT* observations of two distant clusters of galaxies, as well as optical and radio observations of one of them. Both clusters are members of an X-ray–selected sample of clusters of galaxies, a subset of the Extended Medium-Sensitivity Survey (EMSS) (Gioia et al. 1990b; Stocke et al. 1991). One cluster, MS 0735+74, at redshift $z = 0.216$, was found to be a cooling flow candidate based on detection of extended Hα emission in the central brightest galaxy (Donahue, Stocke, & Gioia 1992, hereafter DSG). The other cluster, MS 0451−03, at its newly determined redshift $z = 0.55$ (discussed below), is the most X-ray luminous cluster of galaxies in the EMSS, with an *Einstein* (0.3–3.5 keV) luminosity of 2×10^{45} ergs s^{-1}. We obtained X-ray images and X-ray spectra of both clusters with the *ROSAT* PSPC and HRI. We describe the observations in § 2 and describe the reduction and basic X-ray data analyses with basic results for each cluster in § 3. In § 4 we derive X-ray gas masses and total cluster masses for each cluster. In § 5, we study the cluster shapes and evidence for substructure via elliptical fitting and wavelet analysis. The optical, X-ray, and radio observations of the cooling flow in MS 0735+74 are discussed in § 6. We relate our observations to cluster evolution and summarize results in § 7.

2. THE X-RAY AND OPTICAL OBSERVATIONS

As listed in Table 1, the cluster MS 0735+74 was imaged by the *ROSAT* HRI for 26,933 s and by the *ROSAT* PSPC, which has both imaging and spectral capabilities, for 8782 s. MS 0451−03 was observed with the *ROSAT* PSPC for 16,027 s. All X-ray images contained the extended image of the target cluster in the central 200″ of the field, so off-axis adjustments and exposure corrections were not used.

We obtained red, low-resolution spectra of the central galaxies of both clusters with the Double Spectrograph (Oke & Gunn 1982) at Cassegrain focus of the Palomar 5 m telescope during a night of moderate seeing and poor transparency in 1992 December. We used the 156 lines mm^{-1} grating, which provides a resolution of ∼18.0 Å, and a dispersion of 6.0 Å pixel^{-1}. Wavelength coverage was from the dichroic cutoff at 5500 Å to 1 μm. We also observed MS 0451−03 with Four-Shooter at the prime focus of the Palomar 5 m telescope during a night of poor seeing, Moon, and cloud in 1991 December. A single galaxy provided a reliable redshift of 0.55 and six other galaxies' spectra summed together also gave a redshift of 0.55. This redshift has now been confirmed by the acquisition of a large number of cluster redshifts by the Canadian Network for Observational Cosmology (CNOC) collaboration (see Carlberg et al. 1994) and will be reported later.

All scales and 0.2–2.5 keV luminosities are computed assuming $H_0 = 50$ km s^{-1} Mpc^{-1} and $q_0 = 0.5$. In the following subsections, a King profile is assumed to be $I(r) \propto [1 + (r/r_c)^2]^{-3\beta+(1/2)}$, where r_c is the core radius and β is known as $\beta_{\rm image}$ or $\beta_{\rm fit}$ in the literature. In isothermal models β corresponds to the ratio of kinetic energy in the galaxies to the thermal energy in the gas. We do not have an independent measure of β (or $\beta_{\rm spec}$) since the velocity dispersions for the galaxies of these clusters are yet unknown.

3. X-RAY REDUCTION METHODS AND ANALYSES OF INDIVIDUAL CLUSTERS

We describe the X-ray data reduction techniques used for both clusters in the following section. For X-ray spectra analysis we extracted a circular region of 100″ and 120″ for MS 0451−03 and MS 0735+74, respectively. For the statistical analyses with χ^2 fitting, we determined an annular background region and excluded the bright sources from the background calculation. The area-normalized background was subtracted from the counts in the circular aperture. In the case of the PSPC, energy information or pulse height were binned into spectra for the cluster and background. For the statistical analyses with maximum-likelihood fitting, background counts were included, and we introduced an additional parameter in the spectral fit, the normalization of the X-ray background, whose shape was approximated by 40 keV thermal bremsstrahlung. We used routines in both PROS and in XSPEC,[1] and the results for all methods were indistinguishable within statistical errors. The results quoted are from XSPEC using χ^2 statistical analysis. We restricted our spectral analysis to those channels with sufficient counts, typically pulse-invariant (PI) channels 7–247, binned into 34 spectral bins.[2] XSPEC convolves the specified model with a response matrix and then compares the convolution to the data. We fitted spectra to a redshifted Raymond-Smith thermal model for an isothermal plasma with 30% solar abundances and local interstellar absorption as an additional free parameter. We achieved satisfactory χ^2 fits for these models, so that including an intrinsic absorption component did not improve the fit and was not required. For completeness, we fitted spectra with absorbed power laws. Such fits were not rejected by χ^2 tests. However, both sources are spatially resolved and extremely luminous, and therefore power-law models do not reflect any known physical process.

After fitting a spectrum, we used the best-fit parameters to calculate a conversion from the count rate to an unabsorbed flux. This conversion was used to convert central surface

[1] PROS and STSDAS are data analysis packages found in the Interactive Reduction and Analysis Facility (IRAF). XSPEC is an X-ray spectra analysis package available from the NASA *ROSAT* Guest Observer Facility.

[2] PI bins 7–10, 11–19, 20–31, 32–51, 52–69, 70–90, 91–122, 123–149, 150–179, 180–223, and 224–247 are grouped by factors 2, 3, 4, 5, 6, 7, 8, 9, 10, 11, and 12, respectively.

TABLE 1

X-RAY AND OPTICAL LOG INFORMATION

Target	Telescope	Instrument	Date	Exposure Time (s)
MS 0735+74.....	*ROSAT*	HRI	1994 Mar, Apr	26933
	ROSAT	PSPC	1994 Mar	8782
	Palomar 200	Double Spectrograph	1993 Jan 1	2400
MS 0451−03.....	*ROSAT*	PSPC	1993 Mar	16027
	Palomar 200	Four-Shooter	1991 Dec	3000
	Palomar 200	Double Spectrograph	1993 Jan 1	1200 and 3000

brightness in counts pixel^{-1} to central surface brightness in ergs s^{-1} cm^{-2} arcsec^{-1}.

We extracted a background-subtracted surface brightness profile for each cluster. Since the cluster X-ray shapes were nearly circular, we used circular annular apertures. We fitted the traditional King profile or a King profile with a central Gaussian source to the surface brightness profiles. This approach differs from that of Jones & Forman (1984), who fitted King profiles to only the outer surface brightness points, but it is similar to that described in Henriksen (1986).

For each cluster we fitted its isophotal contours to ellipses with the *isophote* package in STSDAS, based on a method described in Jedrzejewski (1987). We allowed the ellipse center, position angle, and eccentricity to vary at each semimajor axis value. We qualitatively searched for the presence of substructure using a wavelet analysis technique.

We describe and discuss the basic results for the individual clusters below.

3.1. *MS 0735+74*

MS 0735+74 ($z = 0.216$, 4.45 kpc arcsec^{-1}) was identified as a candidate "cooling flow" cluster by DSG because its central galaxy has extended Hα emission and low-ionization emission lines where [O II] λ3727 $\gg$ [O III] λ5007. We confirm this identification with the *ROSAT* HRI detection of a central high surface brightness peak in the central portion of the cluster. Figure 1 (Plate 13) shows the PSPC X-ray surface brightness contours overlaid on a red optical gray-scale image of the cluster galaxies from Gioia & Luppino (1994).

The fitted gas temperature is $2.4^{+2.2}_{-0.8}$ keV ($\Delta\chi^2 = 2.71$, or 90% confidence intervals throughout this paper), assuming 30% metallicity gas and a Raymond model for emission. This temperature is significantly lower than expected for a cluster of its luminosity, given the empirical relationship between L_x and T_x for well-studied X-ray clusters (Mushotzky 1984; Edge & Stewart 1991a; David et al. 1993b). The cooling flow may contribute up to 20% of the emission, given our analysis below of the surface brightness contribution of a putative cooling flow. The corresponding absorption column density is $(3.4 \pm 0.5) \times 10^{20}$ cm^{-2}, not significantly different from the expected Galactic absorption along that line of sight, 3.3×10^{20} cm^{-2} (EINLINE database). The cluster luminosity within 2′ of the center is $6.1 \times 10^{44}\ h_{50}^{-2}$ ergs s^{-1}. A generic absorbed power-law fit with the parameters $N_H = 4.6 \pm 0.9 \times 10^{20}$ cm^{-2} and a rather steep photon index of 1.8 ± 0.3 gave a reduced χ^2 fit of 0.63 with 27 degrees of freedom. The absorbed thermal spectrum gave a reduced χ^2 of 0.52 with 27 degrees of freedom. The thermal spectrum is a better fit, but the power-law model cannot be ruled out by these data. Figure 2 shows the χ^2 contours and model versus data plots for the absorbed Raymond plasma models.

We extracted a radial surface brightness profile of the cluster from both the HRI and PSPC images. We matched the radial profiles in two ways: first by comparing the cluster count rates inside a 2′ radius for both instruments and second by comparing the flux calibration ratio between the HRI and the PSPC for the best-fit spectrum. For both methods we concluded that for this cluster, 1 PSPC count was approximately equal to 3 HRI counts, within about 10%. We then used only the HRI data inside 60″ and the PSPC data outside that radius. (See Fig. 3.) We fitted the radial surface brightness profile to King models and to King models with a Gaussian central source. The fit was significantly improved when we included a Gaussian central source, corresponding to the putative "cooling flow" in the models. We derive a core radius of 234 ± 40 kpc and a β of 0.80 ± 0.25, consistent with those quantities found for clusters of low redshift (e.g., Jones & Forman 1984). The mass cooling rate is $\sim 125\ M_\odot$ yr^{-1}, given the central excess emission and the overall temperature, where $\dot{M} = 2L_{\rm excess}/5kT_x$. The central excess was well fitted by a Gaussian with σ of 6.″6 or $30 \pm 3\ h_{50}^{-1}$ kpc at the cluster. The FWHM of the central Gaussian excess is therefore 15.″5 or $70 \pm 7\ h_{50}^{-1}$ kpc. This is more extended than an HRI point source on axis (David et al. 1993a), so we have resolved the cooling flow region with the *ROSAT* HRI.

3.2. *MS 0451−03*

MS 0451−03 ($z = 0.55$, 7.38 kpc arcsec^{-1}) is the most luminous cluster in the EMSS and, indeed, one of the most luminous clusters known. We show a contour map of the X-ray surface brightness overlaid on an r-band gray-scale image from Gioia & Luppino (1994) in Figure 4 (Plate 14). Since the PSPC is sensitive to low surface brightness emission and has a spatial resolution of $\sim$20″, we have been able to fit a King model with a core radius of 360^{+80}_{-36} kpc and a β of $1.00^{+0.4}_{-0.3}$ to this cluster (Fig. 5.) The cluster luminosity within 100″ is $1.56 \times 10^{45}\ h_{50}^{-2}$ ergs s^{-1}. Notably, the best-fit β parameter is higher than most nearby clusters. Jones & Forman (1984) found a typical β as measured from surface brightness distributions to be $\sim$0.6–0.7. Models by Evrard (1990) suggest that high-redshift clusters might have higher β, according to their simulated X-ray surface brightness profiles.

Spectral fits to Raymond-Smith plasma models and Galactic soft X-ray absorption give hydrogen column densities of $3.2 \pm 0.5 \times 10^{20}$ cm^{-2} and a lower limit for the cluster temperature of 3.5 keV (Fig. 6). With only 1400 detected counts, this cluster is hotter than *ROSAT* can measure. The reduced χ^2 for the best fit was 0.95 for 34 degrees of freedom. An absorbed power law with a photon index of 1.6 and similar absorption column gave an equivalently good fit to the data. This is not surprising since bremsstrahlung from gas hotter than a few keV will look like a power-law spectrum through the *ROSAT*/PSPC bandpass. An emission-weighted gas temperature and iron abundance will be reported for this cluster from *ASCA* observations, which are sensitive to a larger energy range (Donahue & Stocke 1995). This cluster also does not show excess soft X-ray absorption, since the Galactic value is 4.9×10^{20} cm^{-2}. Therefore, neither of these clusters has an indication of strong excess soft X-ray absorption that may be associated with a cooling flow (White et al. 1991) or processes that preferentially occur in distant clusters (Wang & Stocke 1992).

The X-ray appearance of the cluster MS 0451−03 may be similar to the X-ray appearance of Coma. The magnitude of a central cooling flow in MS 0451−03 is under 125 $M_\odot$ yr^{-1}, derived from the upper limit on a central surface brightness excess and the lower limit on gas temperature. While MS 0735+74 seems to be similar in morphology to cooling flow clusters nearby, MS 0451−03, on the other hand, shows a somewhat larger core radius and steeper β, similar to clusters which do not have a dominant central galaxy, such as Coma. Such clusters tend to have larger core radii (Jones & Forman 1984). The X-ray aspects of these clusters are consistent with their optical characteristics. The cooling flow cluster MS 0735+74 has peaked central X-ray emission centered on a dominant central galaxy and a compact X-ray core radius, as

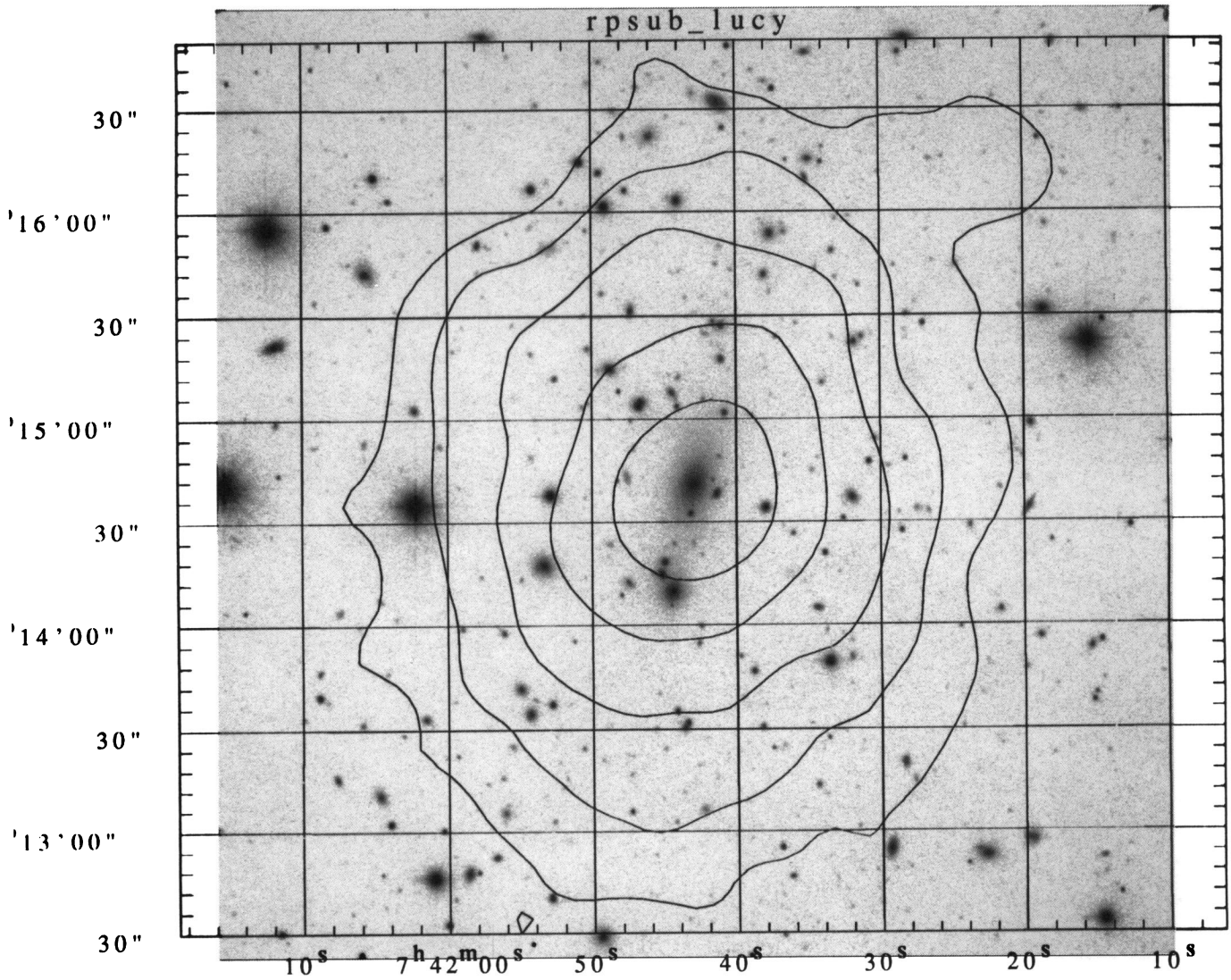

FIG. 1.—A gray-scale of optical red CCD image of MS 0735+74 with the PSPC X-ray surface brightness contours overlaid. The axes are sky coordinates in the epoch J2000. The X-ray contours correspond to unabsorbed surface brightness levels of 0.67, 1.2, 2.2, 4.0, and 7.3 × 10^{-13} ergs s^{-1} $arcmin^{-2}$. The red image was published in Gioia & Luppino (1994).

DONAHUE & STOCKE (see 449, 556)

PLATE 14

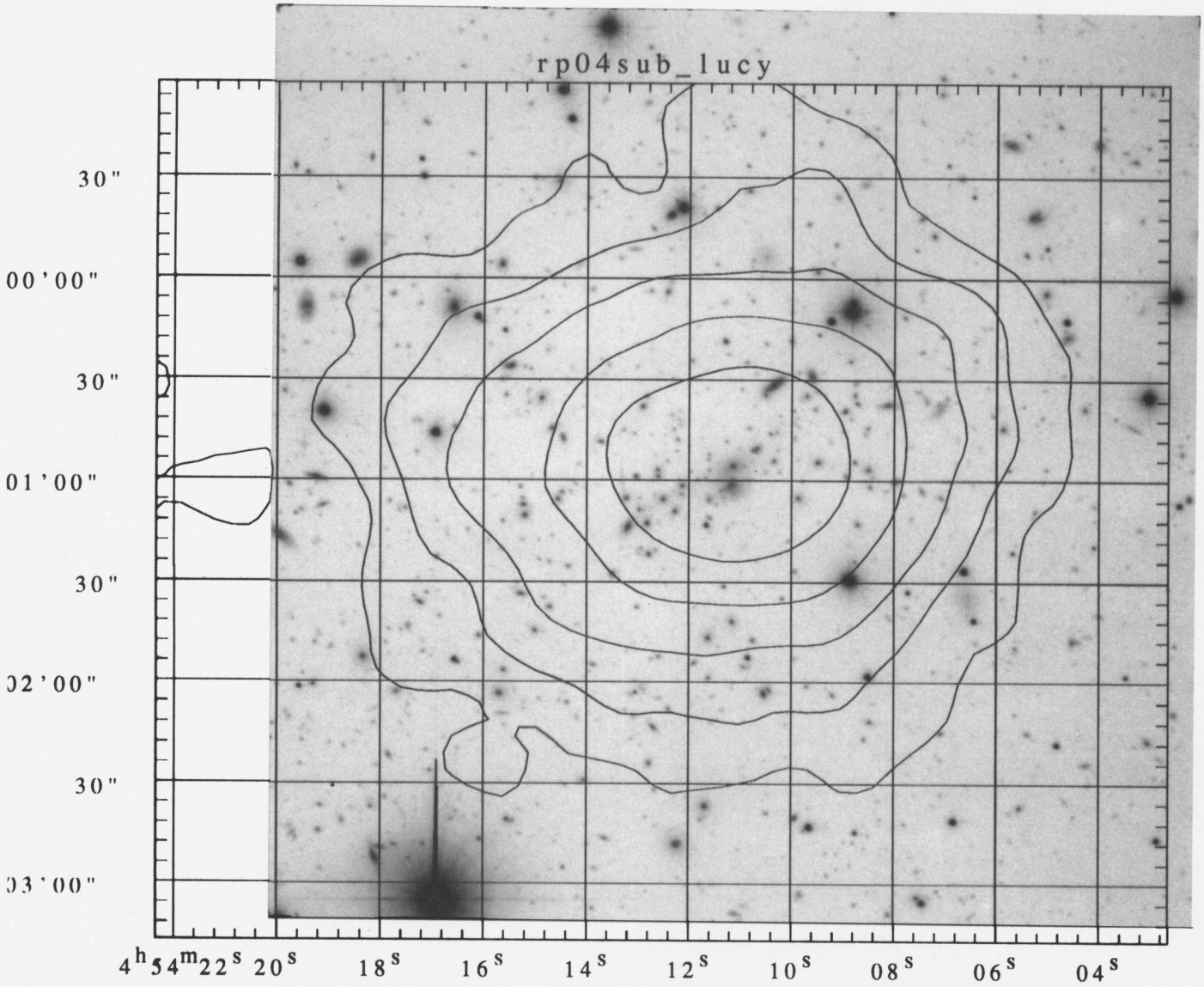

FIG. 4.—The X-ray PSPC surface brightness contours of the cluster MS 0451−03 overlaid on a gray-scale *R*-band CCD image from Gioia & Luppino (1994). The X-ray contours correspond to 0.26, 0.47, 0.86, 1.57, and 2.86 × 10^{-14} erg s^{-1} cm^{-2} $arcmin^{-2}$. The shapes of the X-ray contours roughly trace the orientation and extent of the galaxy distribution. The axes are sky coordinates, epoch J2000.

DONAHUE & STOCKE (see 449, 556)

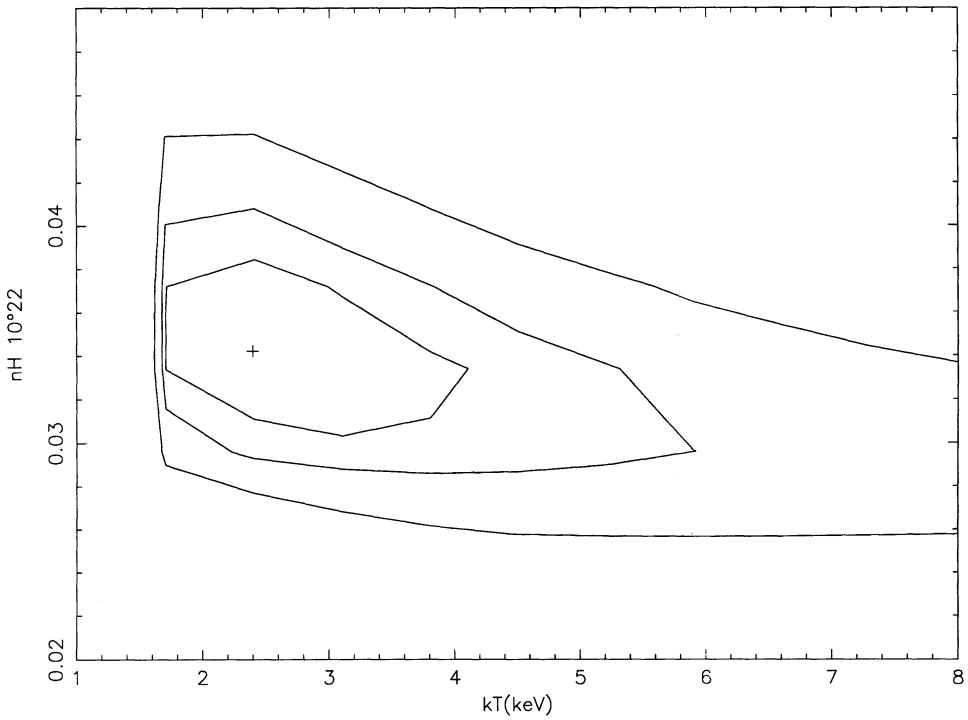

FIG. 2*a*

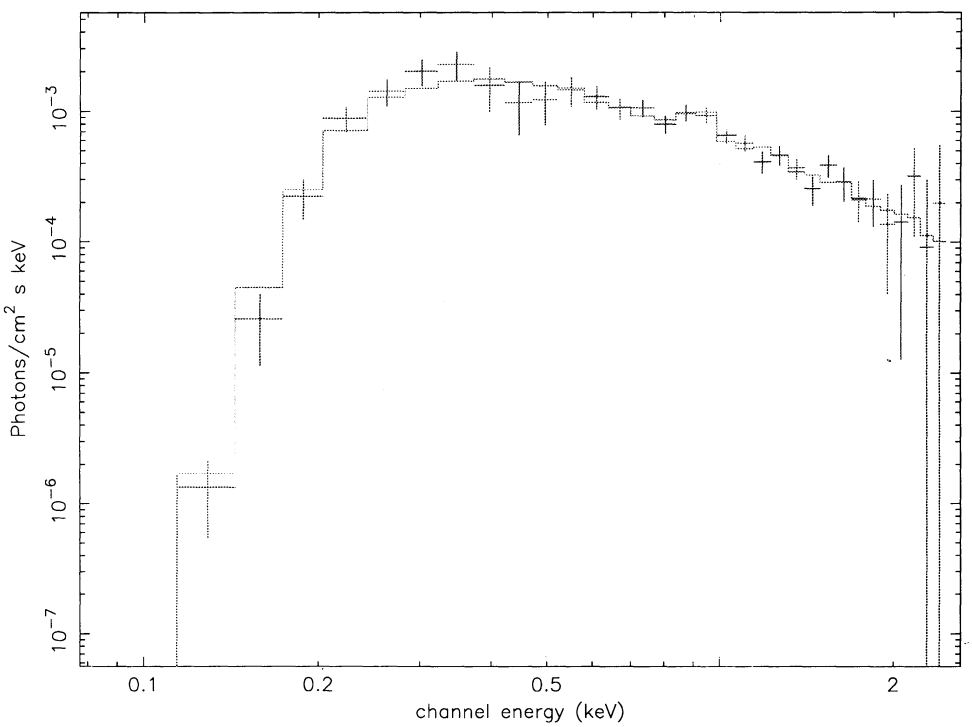

FIG. 2*b*

FIG. 2.—Results of spectral fitting for the PSPC data for MS 0735+74. Fig. 2*a* is a plot of χ^2 contours for the temperature and for the column of X-ray–absorbing material describing an absorbed Raymond-Smith thermal model of a gas with 30% solar metallicity. The X-ray absorption column is scaled to the hydrogen column density with the assumption that the X-rays are absorbed by a solar abundance gas. The contours correspond to $\Delta\chi^2 = 2.30$, 4.61, and 9.21, corresponding to 68.3%, 90%, and 99% confidence levels. Fig. 2*b* shows the fit (line) plotted over the "unfolded" spectrum (histogram), that is, the observed spectrum divided by the response of the spectrograph and telescope.

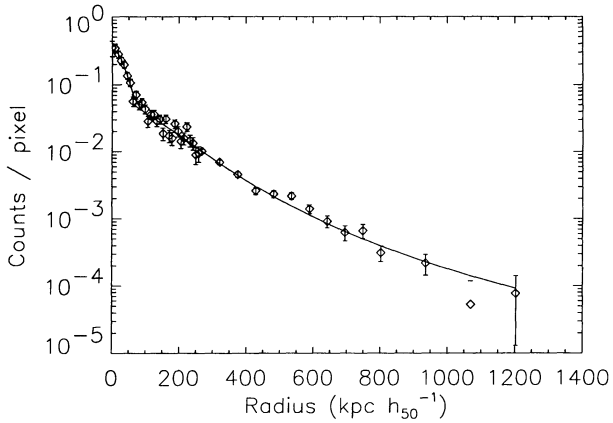

FIG. 3.—Radial plot of the background-subtracted surface brightness in counts pixel^{-1} for MS 0735+74 against radius for data from the HRI and the PSPC (Each pixel is 0.″5 by 0.″5 in angular size.) Data from radii smaller than 60″ (267 kpc h_{50}^{-1}) are from the HRI. A fitted model including a central Gaussian source with a FWHM = 15.″2 or 70 ± 7 h_{50}^{-1} kpc at the cluster redshift and a King profile with a core radius of 234 ± 40 h_{50}^{-1} kpc (52.″6) and $\beta = 0.80 \pm 0.25$ (90% confidence limits) is plotted over the data points. The central Gaussian is clearly more extended than the HRI on-axis point response function, resolving the central cooling region. The excess corresponds to ~125 $M_\odot$ yr^{-1}.

do low-redshift cooling flow clusters. MS 0451−03, which does not have a dominant central galaxy, has a somewhat larger core radius and no evidence for a strong cooling flow, similar to the Coma cluster. However, we describe in the next section how the surface profile distribution and the upper limit to the temperature in MS 0451−03 imply that the gas mass–to–total mass ratio for this cluster is lower than that for nearby clusters, including Coma.

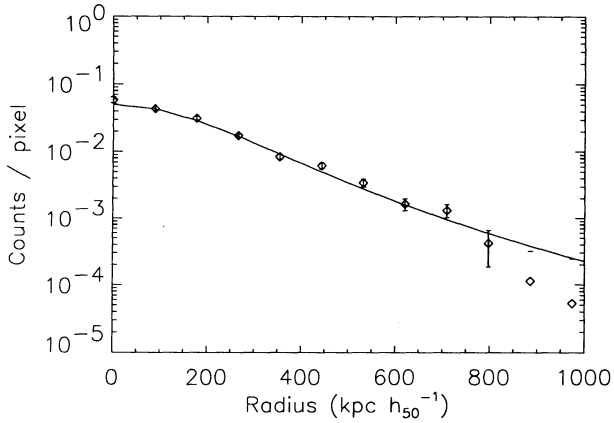

FIG. 5.—The PSPC X-ray surface profile of the cluster MS 0451−03, with background subtracted, in units of counts pixel^{-1} is plotted against radius with the fitted King model overlaid, as in Fig. 3. The fit core radius is 360^{+80}_{-36} h_{50}^{-1} kpc (48.″8) and $\beta = 1.0^{+0.4}_{-0.3}$. Quoted errors are 90% confidence bounds.

4. CLUSTER MASSES AND GAS MASSES

Here we derive a cluster gas mass and the total gravitational mass for each cluster. We estimate the central gas density with the formula given in Henry & Henriksen (1986) and then numerically integrate the gas mass out to a radius (R_{max}) of 1 Mpc h_{50}^{-1} using parameters β and core radius a as derived from the surface brightness fit, such that

$$M_{gas} = \int_0^{R_{max}} \rho_0 [1 + (r/a)^2]^{-3\beta/2} 4\pi r^2 \, dr \, . \quad (1)$$

For comparison to cluster masses in the literature, we estimate a mass within a projected radius by assuming that the

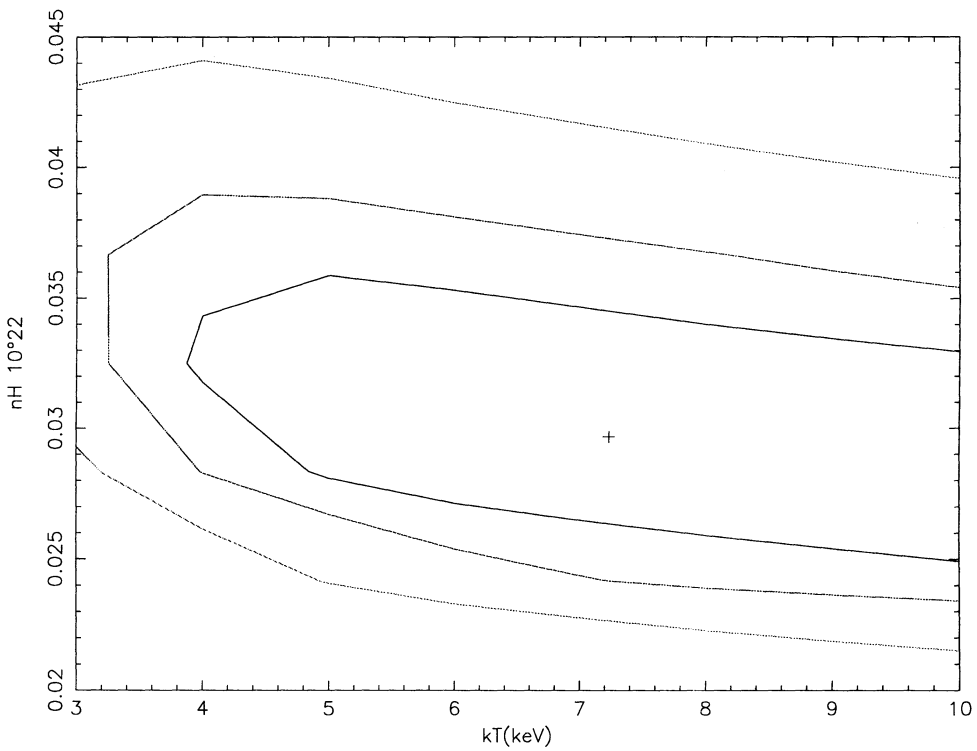

FIG. 6.—The plot of χ^2 contours for the cluster MS 0451−03 X-ray temperature and the X-ray absorption column, as per a fit to a Raymond-Smith model with 30% solar metallicity, as in Fig. 2. The contours correspond to $\Delta\chi^2 = 2.30$, 4.61, and 9.21, corresponding to 68.3%, 90%, and 99% confidence levels. We obtain only a lower limit for T_x for this cluster.

cluster is isothermal and in nearly hydrostatic equilibrium, with the gas density $\propto[1 + (r/a)^2]^{-3\beta/2}$. This method will give us a cluster mass to within a factor of 2 or less (Tsai et al. 1994):

$$M(r) = 10^{14}\ M_\odot\ \beta T(\mathrm{keV}) r(\mathrm{Mpc})\ \frac{(r/a)}{1 + (r/a)^2}\ . \qquad (2)$$

$M(r)$, as well as $M_{\rm gas}$ estimated in this way, diverges with radius. This expression does not apply outside cluster radii of 1–3 Mpc, where the gas may not be in hydrostatic equilibrium, the galaxies might not be virialized, and the X-ray brightness is too low for reliable gas density determination. For these observations, $R_{\rm max} = 1$ Mpc.

Henry & Arnaud (1991) estimate a complete cluster mass by taking the relationship between cluster temperature, formation redshift (which we assume to be the observed redshift), and the cluster mass as normalized by hydrodynamic simulations done by Evrard (1990):

$$M_{\rm cluster} = 2 \times 10^{15}\ M_\odot\ h_{50}\ \frac{kT}{6.4\ \mathrm{keV}}\ (1 + z_f)\ . \qquad (3)$$

However, comparison of the gravitational mass and the gas mass to derive the hot baryonic fraction must be done out to the same cluster radius, since this fraction may vary as a function of radius. To use the expression in equation (3) in estimating the $M_{\rm gas}/M_{\rm cluster}$ fraction, the gas mass should be known out to $R_{\rm max} \geq 3$ Mpc $h_{50}(1 + z_f)/\beta$, if the gas is isothermal. But from recent cluster and group observations, the gas is only nearly isothermal outside the influence of the cooling flow and inside several core radii (David et al. 1994). Theoretical models simulating a cluster ICM by Tsai et al. (1994) also suggest this. Therefore, estimates for the hot baryonic fraction through the outer regions of clusters, for $R_{\rm max}$ larger than several core radii a, must be done with spatially resolved spectral data, which for distant ($z \gtrsim 0.2$) clusters awaits the *Advanced X-Ray Astrophysics Facility I* (*AXAF-I*).

As can be seen from Table 2, we derive a somewhat smaller gas mass–to–total mass (as derived from eq. [2]) ratio internal to 1 h_{50}^{-1} Mpc ($<17\%$) for MS 0451−03 than that which has been observed in nearby clusters (15%–30%). Since we know only the lower limit to the temperature from *ROSAT* observations, the mass ratio derived is an upper limit. If the gas temperature of MS 0451−03 is similar to that predicted by the L_x-T_x relation for local clusters (Edge & Stewart 1991a; David et al. 1993b), $T_x \sim 11$ keV, $M_{\rm cl} \sim 10^{15}\ M_\odot$, and the gas/total ratio is 6%, substantially smaller than that in nearby clusters. The gas/total ratio for MS 0735+74 is typical of clusters nearby (Edge & Stewart 1991a). If T_x for MS 0451−03 is lower than low-redshift clusters of similar luminosity as predicted by models for cluster evolution (e.g., Perrenod 1980) and tentatively suggest by stacking X-ray spectra of moderate-redshift clusters (Henry, Jiao, & Gioia 1994), then the gas–to–total mass ratio for MS 0451−03 is between 6% and 17%.

TABLE 2

DERIVED GAS MASSES AND TOTAL CLUSTER MASSES INSIDE 1 Mpc

Parameter	MS 0735+74	MS 0451−03
Redshift	0.216	0.55
$n_0\ (\mathrm{cm}^{-3})\ h_{50}^{1/2}$	4.3×10^{-3}	3.3×10^{-3}
$M_{\rm gas}\ h_{50}^{-5/2}\ (M_\odot)$	6.4×10^{13}	6.1×10^{13}
$M_{\rm total}\ h_{50}^{-1}\ (M_\odot)$	$2.5^{+2.4}_{-1.1} \times 10^{14}$	$>3.5 \times 10^{14}$
Ratio $h_{50}^{-3/2}$ (gas/total)	25% (13%–46%)	$<17\%$

In agreement with measurements of clusters by *Einstein* and *EXOSAT*, we show that the gas mass–to–total mass ratio for clusters can be high. These observations further suggest that this high ratio persists, at least for luminous X-ray clusters, out to moderate redshifts. If clusters are not excessively baryon rich in comparison to the rest of the universe, then the ratio of gas to dark matter in clusters is approximately the ratio of baryonic to dark matter in the universe. A high ratio implies that a substantial fraction of the matter in the universe is baryonic. This is in conflict with a flat ($\Lambda = 0.0$, $\Omega = 1.0$) universe and the limits on baryonic matter placed by primordial nucleosynthesis calculations where $\Omega_{\rm baryon}\ h_{50}^2 = 0.05 \pm 0.01$ (Walker et al. 1991), as has been noted by other authors (Briel, Henry, & Böhringer 1992; White et al. 1993.)

5. MORPHOLOGY AND SUBSTRUCTURE

5.1. *Isophotal Fitting*

We have made a preliminary attempt to quantify the nonregularity of these high-redshift clusters by fitting elliptical isophotes to the X-ray maps of the clusters using the STSDAS package *isophote*. We used the PSPC maps of the clusters since we can see the clusters out to larger radii in these maps; the HRI map of MS 0735+74 was analyzed as well, but only to probe regions interior to the central arcminute of the cluster. We extracted a subsection of the map and deconvolved it with a Lucy-Richardson algorithm, using the PROS-supplied *ROSAT* on-axis point response functions, smoothing the raw image in a way consistent with the known instrumental response. The Lucy-Richardson algorithm in STSDAS was developed for data reconstruction for the *Hubble Space Telescope*, but it is well suited for X-ray images because the readout noise is zero and the pixel values are photon counts. The only limitation is that we have only on-axis point response functions; however, since these clusters were observed nearly on axis, this limitation does not affect our results significantly. We allowed the centers of the ellipses to vary, as well as the position angle and the ratio of the major and minor semiaxes. Uncertainties in fitted parameters were computed interior to the task *isophote.ellipse* and are obtained from the residual intensity scatter, combined with the internal error in the harmonic fit, after removal of the first and second fitted harmonics (Jedrzejewski 1987). We found no significant deviations from ellipticity (i.e., the coefficients $A3$, $B3$, $A4$, and $B4$ [Jedrzejewski 1987] were statistically consistent with zero). We did not detect significant shifts in the centers of the ellipses (see Figs. 7–9, *bottom two panels*). The only centroid shift seen was in MS 0451−03, where the best-fit center moved $\sim 20''$ to the east of the initial centroid position, but the errors in this determination overlap the initial centroid position.

We find that the position angles of the fitted ellipses do not change with semimajor axis length, except in the case of MS 0735+74, where the position angle of the inner 90 kpc ($20''$) differs from the position angle of the fitted ellipses outside this region. MS 0451−03 has a position angle of $92° \pm 9°$ within a projected semimajor axis of 800 kpc ($100''$), and MS 0735+74 varies from $10°$ to $-40°$ (Figs. 7–9, *upper right panels*). The eccentricity is also roughly constant with radius throughout the clusters, except in the inner $30''$ of MS 0735+74 (Figs. 7–9, *upper left panels*). (We plot the results for the PSPC observations of MS 0735+74 even though the PSPC has poorer

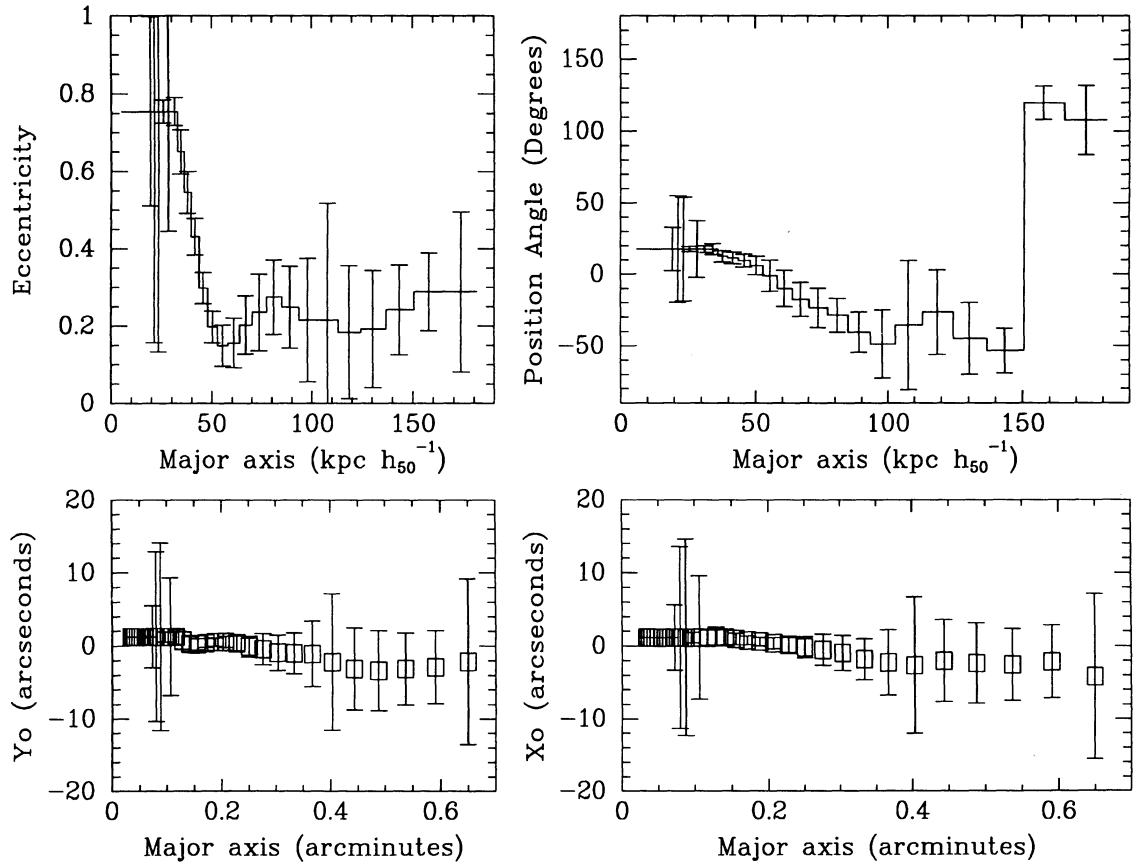

FIG. 7.—Results of fitting ellipses to the Lucy-deconvolved, HRI X-ray surface brightness image of the cluster MS 0735+74, with the STSDAS package stsdas.analysis.isophote.ellipse. The x-axes of the upper plots give the spatial scale; the x-axes of the lower plots give the angular scale for the same points. *Upper left:* Elliptical eccentricity ϵ as a function of semimajor axis. *Upper right:* Position angle, as defined in degrees of east of north. *Lower left and right:* A plot of centroid position difference from the mean centroid position in arcseconds, which was allowed to vary with each fit to elliptical isophotes with semimajor axis length. Y_0 is declination shift in arcseconds; X_0 is the shift in right ascension in arcseconds.

spatial resolution than the HRI and does not reveal the same detail in the central 100 kpc h_{50}^{-1} as the HRI. Since the PSPC is more sensitive to low surface brightness features, it detects the cluster to larger radii.) A centroid shift of about 10″ east to west is measured in the interior 200–300 h_{50}^{-1} for MS 0451−03. Position angle and eccentricity remain nearly constant throughout the detected cluster emission.

For clusters in which only self-similar processes such as gravitational collapse are important, the eccentricity and the position angle of the ellipses should not change with radius. However, the volume where gas is dense enough to cool within the lifetime of the cluster has a characteristic scale known as the cooling radius. Therefore, isophotal ellipses may not be self-similar inside the cooling radius, as seen in MS 0735+74. Even where the cluster X-ray emission traces the gravitational potential, the X-ray isophotes do not have to be round. Ellipsoidal dark matter shapes the emissivity of the hot gas confined within its potential; thus, the X-ray surface brightness contours need not be perfect circles (Buote & Canizares 1992). The galaxies should align with the X-ray gas if their distribution in velocity and space represent the underlying dark matter distribution. This correspondence does not follow for clusters in the process of merging (e.g., A754 discussed in Zabludoff & Zaritsky 1995). We will investigate this in future work in collaboration with optical observers who are accumulating velocity dispersions and galaxy distributions for a sample of EMSS clusters. Interestingly, the fitted elliptical isophotes of both clusters have the same eccentricity, $\epsilon \sim 0.25$.

We created a model image from the fitted ellipse parameters from each cluster and then subtracted that image from the deconvolved image. The HRI image of MS 0735+74 shows no interesting residuals. The residual PSPC image shows some structure on the scale of the resolution of the PSPC, but below the 3 σ level (<10 counts per feature). Two of the features are regular enough to be background point sources or galaxies within the cluster. If these features corresponded to cluster galaxies, their luminosities would be of order 10^{42} ergs s^{-1}. The MS 0451−03 residual image shows some low-level structure in the form of filamentary structures but, once again, near or just below the 3 σ level of significance. Most of these structures are real, but faint, and if they correspond to structures within the cluster, their luminosities are of order 10^{43} ergs s^{-1} or less.

5.2. *Wavelet Analysis*

X-ray maps can be convolved with functions to allow the automatic detection and characterization of structures on a range of scales by using the wavelet transform (Combes, Grossmann, & Tchamitchian 1988). We performed a wavelet decomposition on all three X-ray maps, centered on the clusters, using the method described in Slezak, Bijaoui, & Mars (1990). In the wavelet transform, the signal $s(x, y)$ is convolved with

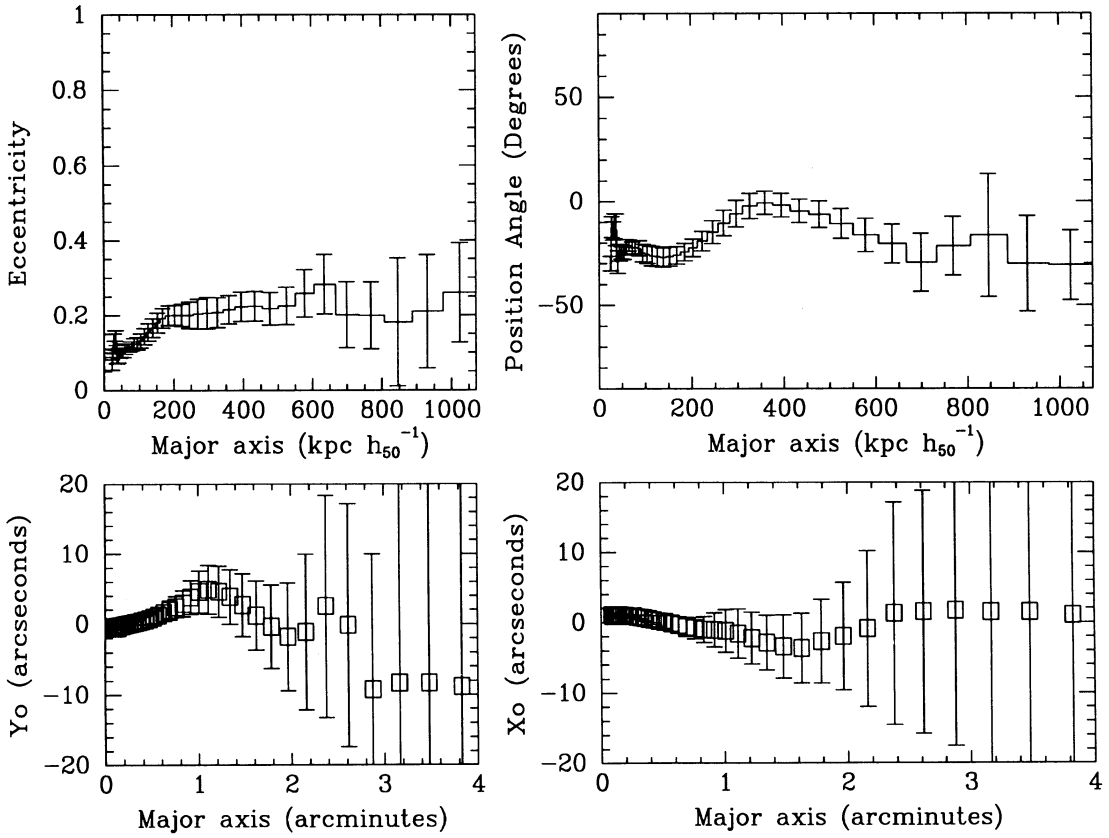

FIG. 8.—Same set of figures producing the results of ellipse fitting to Lucy-deconvolved X-ray surface brightness contours as in Fig. 7, except for the PSPC data for the cluster MS 0735+74. We note that the points interior to the FWHM of the point response function of the PSPC (~0.3) are subject to systematic effects.

respect to the analyzing wavelet $g(x, y)$ which has a zero mean and can be complex valued. The transform $h(x, y, a_x, a_y)$ is a four-dimensional function. For our study we use real, isotropic wavelets, so that $a_x = a_y = a$, and therefore

$$h(x, y, a) = s(x, y) \otimes \frac{1}{a^{1/2}} g\left(\frac{x^2 + y^2}{a^2}\right), \quad (4)$$

where a is the scale of the wavelet. In our analysis, we used a wavelet of a radial Mexican hat,

$$g(x, y, a) = \left(2 - \frac{x^2 + y^2}{a^2}\right) e^{(x^2+y^2)/2a^2}. \quad (5)$$

The Mexican hat wavelet effectively removes flat backgrounds and gradients. We follow the description in Slezak et al. (1990) to compute a wavelet transform image W for a given scale a, as well as V (defined in Slezak et al. 1990). We can then compute the image $Q = W/(V)^{1/2}$. For a statistically uniform distribution, Q is a random variable with a zero mean and unit variance. Slezak et al. (1990) suggest that the significance of fluctuations may be estimated by comparing a histogram of this Q parameter with the Q distribution for a random field containing a similar number of events.

In this exercise, we found that when the wavelet scales were comparable to the size of our 10.7 × 10.7 subimage centered on the cluster, the comparison of the Q-distribution between cluster and background fields were uninformative. One test of this was to compare the Q-distributions of the background fields and, when they started to diverge significantly from each other, to exclude that wavelet scale from comparison. At small scales, the Q-distributions of the background fields did not differ from each other significantly, but the cluster and the background fields did, with extremely high certainty $P \ll 0.0001$. However, this is readily apparent from simple visual inspection of the convolved images.

None of the clusters convolved in this way shows any significant substructure on the scales of 20″–320″. Only the central extended cluster was detected with this method within 5′ of the clusters. This method is a promising one for detecting substructure, particularly when the significance level of a given detection can be quantified. Similar work on a large sample of clusters will reveal whether substructure is more common or more pronounced in clusters at higher redshifts. Applying wavelet analysis to both data and model predictions could provide an additional direct method of comparing the degree of substructure predicted with that observed.

6. A COOLING FLOW IN MS 0735+74

6.1. *Optical Emission Lines*

An optical emission-line nebula exists in MS 0735+74. Such emission-line regions exist in about 40% of X-ray–selected clusters of galaxies (DSG). These nebulae typically extend about 10–100 kpc from the central brightest galaxy in the cluster and are found to be associated exclusively with cluster "cooling flows" (Baum 1992; Heckman et al. 1989).

These nebulae are quite luminous, ranging from 10^{40} to 10^{42} ergs s^{-1} in Hα alone. The total Hα luminosity from MS 0735+74 is 7.33×10^{40} ergs s^{-1} (DSG). The position angle of the optical line-emitting region is not well defined since it is

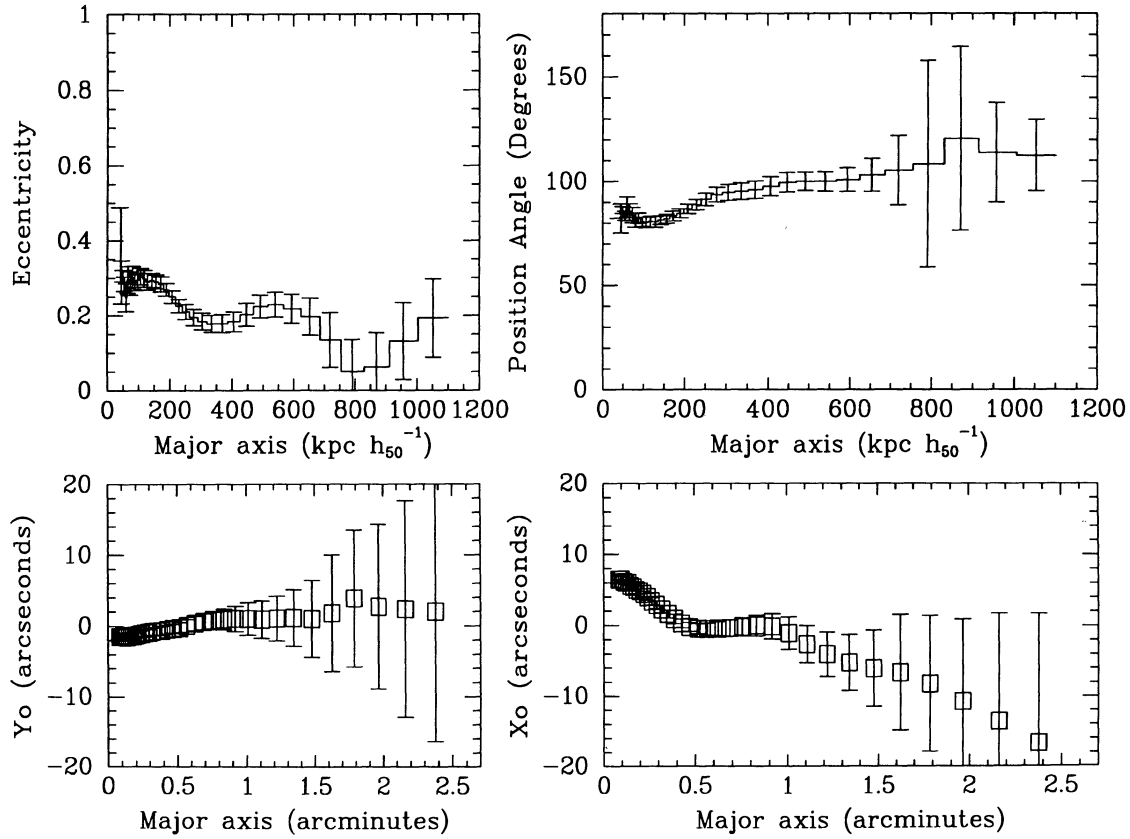

FIG. 9.—Same set of figures producing the results of ellipse fitting to X-ray surface brightness contours as in Fig. 7, except for the cluster MS 0451−03 (PSPC data).

fairly circular; however, there is a slight elongation about 20° east of north at radii of 5″–20″. The HRI image shows that the central 20″ of the X-ray–emitting region is oriented approximately 20° east of north, and a combination of the HRI and the PSPC data shows the isophotes twist outside this region between −30° and 0° east of north (see Figs. 7–8). The twisting of the X-ray isophotes tentatively supports a connection between the X-ray emitting gas and the optical line gas.

If EUV photons from cooling gas are reprocessed into the optical emission from filaments, the maximum Hα–to–X-ray ratio is 0.33 (Donahue & Voit 1991). To test this, the net (continuum-subtracted) Hα image from DSG was degraded to the poorer angular resolution of the *ROSAT* HRI and corrected for contamination by [N II] line emission. We extracted the Hα surface brightness from several radial annuli centered on the brightness cluster galaxy. The ratios of Hα to X-ray surface brightness inside four radial bins are reported in Table 3. We note two things: (1) the surface brightnesses of Hα stay below 3% of the X-ray surface brightness, and (2) the surface brightness ratio decreases with radius. This second trend may be because the filaments have a lower covering fraction with respect to the hot gas at larger radii, because the emitted spectrum of the cooling gas may be more efficiently converted to Hα at smaller radii because the gas is cooler and the emitted spectrum is softer, or because the cooling occurs inhomogeneously, a suggestion consistent with X-ray images of cooling flows at low redshift (see Fabian, Nulsen, & Canizares 1984, 1991).

TABLE 3

Hα/X-RAY SURFACE BRIGHTNESS RATIOS INSIDE FOUR RADIAL BINS

Radius Range (kpc h_{50}^{-1})	Ratio
0–16	0.021 ± 0.004
16–35	0.012 ± 0.002
35–55	0.002 ± 0.001
>55	<0.001

Reduction of the Palomar observations (described in § 2) were done in a standard manner with IRAF procedures. CCD frames were bias subtracted and flattened with dome flats. Spectra were wavelength calibrated with reference arc frames and extracted along the dispersion. The slit width was 2″, and extraction width was ∼4″.

Our long-slit spectra of the central nebula in MS 0735+74 show emission lines typical of "class II" cooling flow nebulae such as those observed in Perseus A (NGC 1275, A426, and 3C 84) or A2597 (Heckman et al. 1989). See Table 4 for the line ratios. The lines were corrected for atmospheric extinction and calibrated to obtain relative fluxes. The third column gives the line ratios corrected for Galactic reddening but not internal reddening. Galactic reddening $E(B_V) \sim 0.06$ for $N_H \sim 3 \times 10^{20}$ cm^{-2}. We assumed $c_{H\beta} = 1.47E_{B-V} = 0.09$, where c is the logarithmic extinction at Hβ (Seaton 1979). The reddening law characterized by Seaton (1979) was used to correct the line ratios. The lines are relatively narrow (<800 km s^{-1}), thus ruling out the existence of a luminous or massive AGN. The raw Hα-to-Hβ ratio in the cluster is 5.0 ± 1.8, significantly

TABLE 4

OPTICAL EMISSION-LINE RATIOS FOR NEBULAE IN MS 0735+74

Flux Ratio (Å)	Raw Flux Ratios	Dereddened Line Ratios
[O II] λ3727/Hα	1.41 ± 0.14	1.61
[O III] λ5007/[O II]	0.15 ± 0.04	0.16
[N II] λ6584/Hα	0.45 ± 0.05	0.45
[S II] λ6716/Hα	0.23 ± 0.05	0.23
[S II] λ6716/[S II] λ6731	2.6 ± 1.5	2.6
Hα/Hβ	5.0 ± 2.0	4.7
[O III] λ5007/Hβ	1.2 ± 0.5	1.2
[O III] λ5007/Hβ[a]	0.59	...

[a] Assuming that Hα/Hβ = 2.86.

larger than case B recombination (2.86) and somewhat larger than ratios (up to 4.0) predicted by photoionization models that reproduce the red emission-line ratios (Voit, Donahue, & Slavin 1994), so dust may lie along the line of sight to the nebulae or mixed in the nebular gas, as suggested by Donahue & Voit (1993) for several low-redshift emission-line filaments in cooling flows. The Hβ flux is uncertain because the redshifted line lies in a very noisy portion of the spectrum (both instrumental and sky noise) and because the stellar absorption at Hβ in the host galaxy probably has comparable absolute equivalent width to that of the detected Hβ emission.

6.2. *Radio Map of MS 0735+74*

The field of MS 0735+74 was observed with the VLA in its standard A configuration on 1992 December 1 for a single 7 minute snapshot at 1425 MHz. A cleaned contour map of the inner 12″ of the field of view is shown in Figure 10. The lowest contour level is shown is at 3 times the map rms noise level.

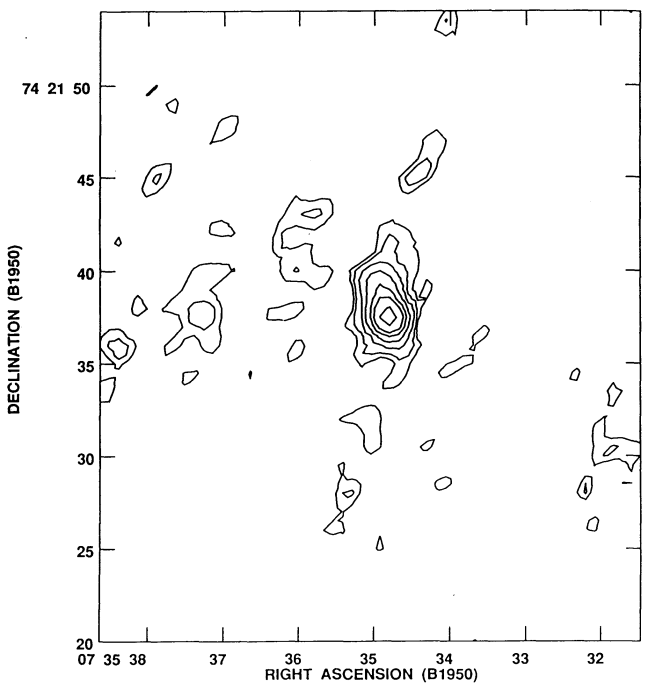

FIG. 10.—A 1.4 GHz map of 4C 74.13, the central radio source in the cooling flow cluster MS 0735+74. The peak flux is 2.1 mJy beam^{-1}, and the total observed flux in this source is 4.4 mJy. Contour levels are at 6×10^{-5} Jy × (−3, 3, 5, 8, 16, 32), where the base level is the rms in the map. The radio source is elongated at 10°, nearly at the same angle as the optical emission-line region.

Like most central radio sources associated with cooling flow clusters (e.g., Ball, Burns, & Loken 1993), this source has an amorphous morphology and a steep spectrum. Previously, Slingo (1974) presented two frequency observations (408 and 1407 MHz) made with the Cambridge 1 mile telescope which yielded a spectral index of 1.7 for this source (also called 4C 74.13). Like Figure 10, the 408 MHz map of 4C 74.13 shows an elongated but otherwise undifferentiated morphology at a position angle of 10° extending over 3′. This position angle is similar to that of the optical emission-line region but extends over a much larger volume. The larger scale X-ray emission and the radio emission are nearly cospatial and are oriented in similar directions.

There is one discrepancy between the newer observations of 4C 74.13 and those of Slingo (1974). Whereas the 1407 MHz flux of this source reported by Slingo was 0.04 ± 0.01 Jy, the total map flux in Figure 10 is only 4.4 mJy. Experiments with tapering the A configuration data fail to find more flux in the map than this amount, and an earlier C configuration map (reported in Stocke et al. 1991 and Gioia & Luppino 1994) also finds a flux comparable to that which is seen in Figure 10. If the newer 1.4 GHz flux for this source is used with the previous 408 MHz flux, the revised spectral index is 3.5. Whatever the resolution, this discrepancy underscores the steep-spectrum, amorphous nature of the radio source associated with this massive cooling flow.

6.3. *Spatial X-Ray Spectral Analysis: Effect of a Cooling Flow on Temperature Determination and Temperature/Column Density Radial Variation*

MS 0735+74 has lower temperature than expected from the locally determined L_x-T_x relationship (Mushotzky 1984; Edge & Stewart 1991a). This may arise from effects of the cooling flow (Fabian et al. 1994b). *ROSAT* is more sensitive than previous X-ray experiments to the soft X-ray photons emitted by a cooling flow in clusters, and therefore these photons may be dominating the spectral fit with respect to the hotter gas outside the cooling flow. Since the central excess from the cooling flow is only 20% of the total cluster emission, it should not dominate the total spectrum. We examine how the cooling flow affected the overall cluster temperature in two ways: (1) simulation of cluster spectra and (2) analysis of spectra from two radial bins.

We simulated cluster spectra for a cluster with the same flux as MS 0735+74, a redshift of 0.216, a cooling flow of 125 $M_\odot$ yr^{-1}, a Raymond-Smith plasma at kT = 3.4 keV, and a PSPC observation of 8800 s. Fitting such spectra with a simple Raymond-Smith plasma produced temperatures and column densities that were 10% lower than that used to generate the models originally. Therefore, the temperature uncertainty is not dominated by the influence of cooler gas in the cooling flow in MS 0735+74 over the statistical uncertainty in the data.

We divided the actual source counts from MS 0735+74 into three spectra: a central spectrum comprising only the counts within 60″ from the center, a total spectrum of the counts within 120″ of the center, and an outer spectrum composed of the counts extracted from an annulus between 60″ and 120″. The results of spectral fitting to a thermal Raymond-Smith spectrum with 30% cosmic abundances, redshifted to z = 0.216 and restraining the fit to energy bins between 0.08 and 2.2 keV, are reported in Table 5. The errors reported are $\Delta\chi^2$ = 2.71 or 90% confidence limits. The total spectrum is thus also consis-

TABLE 5

SPATIAL TEMPERATURES FROM MS 0735+74

Parameter	Center 60″	Total 120″	Outer 60″–120″
Total Counts	1336 ± 43	2023 ± 53	687 ± 34
T_x (keV)	$2.4^{+2.2}_{-0.8}$	$3.5^{+3.3}_{-1.3}$	>2.2
$N_H/10^{20}$ cm^{-2}	3.4 ± 0.5	$2.9^{+0.4}_{-0.3}$	<3.2
χ^2_{red}	0.59	0.65	0.41

NOTE.—See text for description of apertures.

tent with cooler and somewhat more strongly absorbed (although still consistent with the Galactic value) gas in the central cooling flow of MS 0735+74. In comparisons between the spectra from different projected regions of the cluster, the most significant difference is in the measured column density, with the highest absorption measured in the center of the cluster. For the outer rim of the cluster, the 90% confidence upper limit to the absorbing hydrogen column is 3.2×10^{20} cm^{-2}, whereas in the center the 90% confidence limit for the absorbing column of gas is $3.4 \pm 0.5 \times 10^{20}$ cm^{-2}. The best-fit temperatures indicate that the gas may be somewhat cooler in the center, but the 90% confidence intervals overlap significantly. A comparison of the unfolded spectrum (data with the PSPC response divided out) shows a significant excess of soft X-rays coming from the outer annuli of the cluster. This excess corresponds to an excess column density in the center of only a few $\times 10^{19}$ cm^{-2}. Converting this into an absorbing mass, $M_{abs} \sim 2.5 \times 10^{10}\ M_\odot\ h_{50}^{-2}$ for a solar metallicity gas. The assumption of metal abundances lower than solar increases the required absorbing mass. If this gas is the product of cooling, the magnitude of the absorption implies that the cooling has been occurring at the present rate for only $\sim 2 \times 10^8$ yr. The central absorption is significantly less than that which may have been observed in nearby cooling flow clusters (White et al. 1991; Arnaud et al. 1992a; Fabian et al. 1994a).

For PSPC spectra of thermal emission from hot gas, we cannot independently measure metallicity and column density. These two parameters are impossible to decouple with the poor spectral resolution of the *ROSAT* PSPC. So, for completeness, the differences in the soft X-ray bins of the radial spectra can also be reproduced if there is a metallicity gradient of primordial abundances (no metals) in the cluster outskirts to 30% solar abundances in the center, with the column density fixed at the Galactic value. However, there is no statistical constraint on the metallicity in the outermost bin.

6.4. *Cooling Flows and Excess Absorption*

By identifying a central excess of X-ray emission in the cluster MS 0735+74, we have been able to confirm one of the high-redshift cooling flow candidates of DSG. The primary conclusion of DSG was that cooling flows exist at high redshift and are common in X-ray–luminous clusters (nearly 40% of the X-ray–selected clusters in the sample had the characteristic of extended Hα from their central galaxy). This study also suggested that cooling flows with optical emission-line nebulae might be somewhat more common at high redshift than at low. However, since DSG was a survey of a flux-limited sample, we must not exaggerate this last result. If cooling flow nebulae are found preferentially in the most luminous clusters, then the fraction of clusters with optical emission-line filaments in a flux-limited survey may increase with distance from the observer. The number of clusters in the survey was not sufficient to test this possibility. A similar search for extended Hα emission done for the clusters in the larger *ROSAT* All-Sky Survey will eventually have sufficient numbers of objects to do a statistical evaluation of the suggestion of DSG.

The other issue relevant to cooling flows is the presence of soft X-ray absorption. White et al. (1991) in *Einstein* SSS spectra, Arnaud et al. (1992a) with BBXRT spectra, and Fabian et al. (1994a) in *ASCA* spectra detected absorption in excess of Galactic absorption along the line of sight to cooling flow clusters of order $N_H \sim 5 \times 10^{20}$ cm^{-2}. Since this material has to have a fairly high covering fraction to be detected in the wide-angle X-ray experiments, the amount of absorbing material is quite large: $\sim 3 \times 10^{11}\ M_\odot\ N_{excess}\ R_{100}^2$, where N_{excess} is in units of 10^{21} cm^{-2} and R_{100} is the size of the cold material in units of 100 kpc. As we discussed earlier, the PSPC spectra of counts from separate spatial regions in the cluster MS 0735+74 show evidence for a somewhat larger absorption component in the cluster center than in the outskirts, but the excess in this cluster is only of order $\sim 10^{19}$ cm^{-2} However, higher resolution BBXRT and *ASCA* spectra of the centers of cooling flow clusters have required a cooling flow spectral component in order to fit line emission in cluster X-ray spectra. Since this extra component adds soft X-ray photons to the intrinsic spectrum, additional absorption is required to fit these observations. The *ROSAT* PSPC does not have the spectral resolution to detect line emission from clusters, and therefore a cooling flow component is not required to fit the data adequately. More high-resolution spectra will show whether all cooling flow clusters show absorption, and whether this trait is correlated with the magnitude of the cooling flow. Intrinsic absorption could trace the amount of material that has cooled in the flow at large radii; "young" cooling flows may not have as much material as persistent, long-lived cooling flows.

Wang & Stocke (1992) suggested that distant clusters may have strong soft X-ray absorption, of $\sim 10^{22}$ cm^{-2}, on the basis of stacked IPC spectra. If this were true, we may have had difficulty detecting these clusters with *ROSAT*! However, we do not detect strong excess soft absorption in either of these clusters. Similarly, MS 0016+16, the individual detection reported in Wang & Stocke, does not show any excess absorption in *ROSAT* PSPC (J. Hughes, private communication). There is uncertainty in the calibration of the IPC soft X-ray channels that may have affected the results of IPC observations of MS 0016+16 and other distant clusters. Further, the number of counts in the IPC spectra was not very high ($\sim$300 counts).

In conclusion, we have studied this distant cooling flow in many different ways, and we have found no statistically significant difference between it and nearby cooling flows. This suggests that the mechanism for illuminating the nebular gas and the cooling flow physics for production of the X-ray core emission does not change with redshift, at least for the most dramatic and luminous systems. The spatial comparison of the emission-line region and the X-ray–emitting core of MS 0735+74 shows weak correspondence, suggesting that the X-ray plasma and the emission-line nebula might be related. The emission-line ratios are similar to those of "class II" (Heckman et al. 1989) cooling flow nebulae. The orientation of the interior radio emission and that of the optical nebulae are similar on scales smaller than 1′, and the radio contours align roughly with the X-ray contours on larger scales, which suggests that the X-ray, radio, and emission-line plasmas may be

responding to each other or to similar cues from the cluster environment.

7. SUMMARY AND CONCLUSION

With moderate exposure times sufficient to obtain ~ 2000 counts, we have measured an overall temperature for MS 0735+74 and a significant temperature lower limit for the hotter cluster MS 0451−03, as well as core radii, the β parameter, and cooling flow contributions. The main result of this paper is that X-ray–luminous clusters at redshifts of $z \sim 0.2$–0.5 are not dramatically different from similar clusters at nearby redshifts. Their morphologies can be approximated by King models of surface brightness measurements in roughly circular annuli, which produce good χ^2 fits. MS 0735+74 is similar in structure to local "cooling flow" clusters with central dominant galaxies; MS 0451−03 bears a resemblance to a relaxed Coma-like cluster, with no cooling flow or single dominant galaxy. Furthermore, more detailed analyses with elliptical fits and wavelet analyses show no sign of obvious substructure; we can conclude that these are single regular clusters without significant infall of clusters with masses within an order of magnitude or two of the main cluster. Therefore, while substructure and clumpiness could still be present at some level, such irregularities are not much more obvious at high redshift than they were for regular, single, X-ray–luminous clusters at low redshift as observed by earlier X-ray experiments. This is not to say that irregularities do not exist in these objects but, rather, that any existing irregularities are not large (of order 1% of the main cluster luminosity or less).

These two clusters do deviate from local clusters in ways that may indicate evolution. *ROSAT* PSPC observations indicate that MS 0735+74 may be "cool" for its luminosity compared to the ($z \approx 0$) L_x-T_x relation (Mushotzky 1984; Edge & Stewart 1991a). The *upper* limit on the ratio of gas mass to total mass in the central 1 h_{50}^{-1} Mpc of MS 0451−03 is lower than $M_{\rm gas}/M_{\rm cluster}$ in nearby clusters of similar X-ray luminosity. The temperature of this cluster will be better constrained by *ASCA* measurements (Donahue & Stocke 1995). These are, of course, only two clusters, and a complete sample of high-redshift clusters must be studied to confirm and to characterize evolution of the physical properties of X-ray clusters.

Simulations and empirical fits attempting to explain the evolution seen in the EMSS cluster sample predict that massive clusters at high redshift might have smaller X-ray cores, lower temperatures, and less hot gas per unit mass (Evrard & Henry 1991). For example, gas preheated before infall maintains a constant entropy (Kaiser 1991; Evrard & Henry 1991). Such "preheating" models reproduce the evolution seen in the EMSS sample. However, simulations predict the aggregate properties of samples of clusters, rather than the particular properties of individual clusters. The conclusions we can draw from our two high-redshift clusters are somewhat limited, but we can interpret the existence of "normal" luminous clusters at high redshift in two ways: (1) These clusters began their collapse earlier, are more mature than other clusters at the same redshift, and will grow more slowly from now on; or (2) these clusters are the same age as, but more luminous than, other clusters and will grow to be more massive than Coma. The morphologies of these two high-redshift clusters do not exhibit extreme clumpiness, which might be expected if the clusters were very young, so the interpretation we favor at the present is the first one. There may be no special epoch for the formation of clusters; the gravitational collapse that results in structures of similar masses may begin at a range of epochs, rather than at a single time. Deep HRI images of distant clusters would resolve clumpiness inside the cluster core, and temperature measurements of distant clusters would enable us to tell whether such clusters are simply Coma-like systems at redshifts of 0.5.

Finally, "cooling flow" clusters can be identified by their extended Hα emission.[3] At least for one moderate-redshift cluster (MS 0735+74) cooling flow, there is statistically significant increased absorption toward the center of the cooling flow as opposed to the cluster outskirts, corresponding to a modest absorbing mass of $\sim 2.5 \times 10^{10}\ M_\odot\ h_{50}^{-2}$ and an absorbing hydrogen column of $\sim$a few 10^{19} cm^{-2}. Distant clusters probably do not have systematically more intrinsic soft absorption column than nearby clusters.

M. D. was supported by a Carnegie Fellowship and NASA *ROSAT* grant NAG 5-2021. M. D. acknowledges the use of Palomar 5 m telescope and Double Spectrograph instrument to obtain long-slit spectra of the brightest cluster galaxy in both clusters. Simon Morris observed MS 0451−03 with Four-Shooter on the Hale telescope and provided us redshifts for MS 0451−03. (This cluster has been subsequently observed and confirmed in redshift by the Canadian Network for Observational Cosmology [CNOC]). J. T. S. acknowledges NSF grant AST 90-20008 for support of ground-based observations of extragalactic objects at the University of Colorado. The authors thank Eric Perlman for radio map analysis and assistance with the acquisition of radio data. The authors are grateful to Jeffrey Breen for the use of his wavelet analysis code. Isabella Gioia and Gerry Luppino kindly provided PostScript images of their optical data for both clusters. We used the *Einstein* On-Line Service, Smithsonian Astrophysical Observatory, to obtain Galactic neutral hydrogen column densities toward these clusters.

[3] Bright, extended Hα in X-ray clusters may not be present in *all* cooling flows, however. For example, the central galaxy in the Abell cluster A2029 has no detected Hα (Hu, Cowie, & Wang 1985) $< 2 \times 10^{-17}$ ergs s^{-1} cm^{-2} arcsec^{-2} or Hβ (Johnstone, Fabian, & Nulsen 1987) $< 3 \times 10^{-17}$ ergs s^{-1} cm^{-2} arcsec^{-2} emission, yet X-ray data consistently suggest a strong cooling flow (see Sarazin, O'Connell, & McNamara 1992.)

REFERENCES

Arnaud, K. A., et al. 1992a, in Frontiers of X-Ray Astronomy, ed. Y. Tanaka & K. Koyama (Tokyo: Universal Academy), 481
Arnaud, M., Rothenflug, R., Boulade, O., Vigroux, L., & Vangioni-Flam, E. 1992b, A&A, 254, 49
Ball, R., Burns, J., & Loken, C. 1993, AJ, 105, 53
Baum, S. A. 1992, PASP, 104, 848
Briel, U. G., Henry, J. P., & Böhringer, H. 1992, A&A, 259, L31
Buote, D. A., & Canizares, C. R. 1992, ApJ, 400, 385
Burns, J., Rhee, G., Roettiger, K., Pinkney, J., Loken, C., Owen, F., & Voges, W. 1994, in The First Stromlo Symposium: The Physics of Active Galaxies, ed. G. Bicknell, M. Dopita, & P. Quinn (ASP Conf. Ser., 54), 355
Carlberg, R. G., et al. 1994, JRASC, 88, 39
Combes, J. M., Grossmann, A., & Tchamitchian, P., ed. 1988, Wavelets (Berlin: Springer)
David, L. P., Forman, W., & Jones, C. 1990, ApJ, 380, 39
David, L. P., Harnden, F. R., Jr., Kearns, K. E., & Zombeck, M. V. 1993a, The *ROSAT* High Resolution Imager (HRI) (Harvard Smithsonian CfA document)
David, L. P., Jones, C., Forman, W., & Daines, S. 1994, ApJ, 428, 544
David, L. P., Slyz, A., Jones, C. Forman, W., & Vrtilek, S. D. 1993b, ApJ, 412, 479
Donahue, M., & Stocke, J. T. 1995, in preparation

Donahue, M., Stocke, J. T., & Gioia, I. M. 1992, ApJ, 385, 49 (DSG)
Donahue, M., & Voit, G. M. 1991, ApJ, 381, 361
———. 1993, ApJ, 414, 417
Edge, A. C., Stewart, G. C., Fabian, A. C., & Arnaud, K. A. 1990, MNRAS, 245, 559
Edge, A. C., & Stewart, G. C. 1991a, MNRAS, 252, 414
———. 1991b, MNRAS, 252, 428
Evrard, A. E. 1990, ApJ, 363, 349
Evrard, A. E., & Henry, J. P. 1991, ApJ, 383, 95
Fabian, A. C., Arnaud, K. A., Bautz, M. W., & Tawara, Y. 1994a, ApJ, 436, L63
Fabian, A. C., Crawford, C. S., Edge, A. C., & Mushotzky, R. F. 1994b, MNRAS, 267, 779
Fabian, A. C., Nulsen, P. E. J., & Canizares, C. R. 1984, Nature, 310, 733
———. 1991, Astron. Ap. Rev., 2, 191
Gioia, I. M., Henry, J. P., Maccacaro, T., Morris, S. L., & Stocke, J. T. 1990a, ApJ, 356, 35
Gioia, I. M., & Luppino, G. 1994, ApJS, 94, 583
Gioia, I. M., Maccacaro, T., Schild, R. E., Wolter, A., & Stocke, J. T. 1990b, ApJS, 72, 567
Heckman, T. M., Baum, S. A., van Breugel, W. M., & McCarthy, P. 1989, ApJ, 338, 48
Henriksen, M. 1986, Ph.D. thesis, Univ. of Maryland
Henry, J. P., & Arnaud, K. A. 1991, ApJ, 372, 410
Henry, J. P., Gioia, I. M., Maccacaro, T., Morris, S. L., & Stocke, J. T. 1992, ApJ, 386, 408
Henry, J. P., & Henriksen, M. J. 1986, ApJ, 301, 689
Henry, J. P., Jiao, L., & Gioia, I. M. 1994, ApJ, 432, 49
Hu, E. M., Cowie, L. L., & Wang, Z. 1985, ApJS, 59, 447
Jedrzejewski, R. I. 1987, MNRAS, 226, 747
Johnstone, R. M., Fabian, A. C., & Nulsen, P. E. J. 1987, MNRAS, 224, 75
Jones, C., & Forman, W. 1984, ApJ, 276, 38
Kaiser, N. 1991, ApJ, 383, 104
Mushotzky, R. 1984, Phys. Scripta, T7, 157
Oke, J. B., & Gunn, J. E. 1982, PASP, 94, 586
Perrenod, S. C. 1980, ApJ, 236, 373
Roettiger, K., Burns, J., & Loken, C. 1993, ApJ, 407, L53
Sarazin, C. L., O'Connell, R. W., & McNamara, B. R. 1992, ApJ, 389, L59
Seaton, M. J. 1979, MNRAS, 187, 73P
Slezak, E., Bijaoui, A., & Mars, G. 1990, A&A, 227, 301
Slingo, A. 1974, MNRAS, 168, 307
Stocke, J. T., Morris, S. L., Gioia, I. M., Maccacaro, T., & Schild, R. 1991, ApJS, 76, 813
Thomas, P. A., & Fabian, A. C. 1990, MNRAS, 246, 156
Tsai, J. C., Katz, N., & Bertschinger, E. 1994, ApJ, 423, 553
Voit, G. M., Donahue, M., & Slavin, J. 1994, ApJS, 95, 87
Walker, T. P., Steigman, G., Schramm, D. N., Olive, K. A., & Kang, H. S. 1991, ApJ, 376, 51
Wang, Q. D., & Stocke, J. T. 1993, ApJ, 408, 71
White, D. A., Fabian, A. C., Johnstone, R. M., & Mushotzky, R. F. 1991, MNRAS, 252, 72
White, S. D. M., Navarro, J. F., Evrard, A. E., & Frenk, C. S. 1993, Nature, 366, 429
Wise, M. W., & Sarazin, C. L. 1993, ApJ, 415, 58
Zabludoff, A. I., & Zaritsky, D. 1995, ApJ, in press